AIP | Review of Scientific Instruments

Measurement of salinity distributions in salt-stratified, double-diffusive systems by optical deflectometry

T. L. Bergman, D. R. Munoz, F. P. Incropera, and R. Viskanta

Citation: Review of Scientific Instruments **57**, 2538 (1986); doi: 10.1063/1.1139107
View online: http://dx.doi.org/10.1063/1.1139107
View Table of Contents: http://scitation.aip.org/content/aip/journal/rsi/57/10?ver=pdfcov
Published by the AIP Publishing

Measurement of salinity distributions in salt-stratified, double-diffusive systems by optical deflectometry

T. L. Bergman

Department of Mechanical Engineering, University of Texas at Austin, Austin, Texas 78712

D. R. Munoz, F. P. Incropera, and R. Viskanta

Heat Transfer Laboratory, School of Mechanical Engineering, Purdue University, West Lafayette, Indiana 47907

(Received 21 May 1986; accepted for publication 5 June 1986)

Reliable salinity measurements in double-diffusive thermohaline solutions are necessary to understand relevant system behavior. An optical technique, which has previously been used to investigate solute diffusion in isothermal systems, is employed to measure the salinity distribution in a double-diffusive thermohaline system. The technique is verified by comparison with independent salinity measurements, and its use in a double-diffusive system reveals detailed salinity distribution information. When used with the shadowgraph method of flow visualization, the salinity measurement technique permits a more quantitative interpretation of the shadowgraphic results.

INTRODUCTION

Accurate evaluation of salinity distributions in double-diffusive thermohaline systems[1] is necessary to understand phenomena responsible for system behavior. A variety of salinity measurement techniques, ranging from simple fluid extraction/weight analysis[2] to schemes involving electroconductivity probes,[3] have been developed. Unfortunately, these methods are characterized by limitations in their sensitivity or range of application. For example, the spatial resolution of the extraction method is unknown and real-time salinity measurement is impossible. Difficulties associated with electroconductivity probes may, in general, be traced to electrode surface degradation and are discussed elsewhere.[4]

Because of the uncertainties and/or difficulties associated with fluid extraction or electrical measurement of salinities, various optical techniques have also been used. These techniques include shadowgraphic,[5] interferometric,[6] and fiber-optic refractometric[4] methods. The first two schemes involve observation of the effects of spatial variations in the fluids' refractive index, while the third scheme involves direct measurement of the refractive index. However, these techniques are also characterized by various limitations. For example, the shadowgraph can be used in a qualitative manner to locate regions where changes in the salinity (refractive index) gradient occur, but quantitative interpretation of shadowgraphs is more difficult. Interferometry involves cumbersome procedures which are susceptible to potentially serious refraction error,[7] and although the newer fiber-optic technique shows promise, the refractometer design has not been optimized.

Clearly, several options are available to monitor salinity conditions in double-diffusive thermohaline systems. However, the established techniques may not be suitable for use in a particular experiment. As such, it is useful to consider alternative measurement schemes for nonintrusively determining salinity in double-diffusive thermohaline systems.

The first objective of the present study is to develop a methodology for using the optical deflectometry technique[8,9] in double-diffusive systems. The second objective is to utilize simultaneous deflectometric salinity measurements and shadowgraph flow visualization to provide a more quantitative interpretation of shadowgraphic results.

I. EXPERIMENTAL TECHNIQUES

Experimental investigations of salt-stratified, double-diffusive systems generally involve the thermal destabilization of a salt-stratified fluid layer by bottom heating.[1,10] As shown in Fig. 1, the unstable temperature distribution can induce a bottom mixed layer, which grows at the expense of fluid entrained from the overlaying stable region. The stabilizing salinity distribution suppresses upward growth of the bottom mixed layer, which is characterized by nearly uniform temperatures and salinities. The system may be approximated as having one-dimensional salinity, temperature, and refractive index distributions.

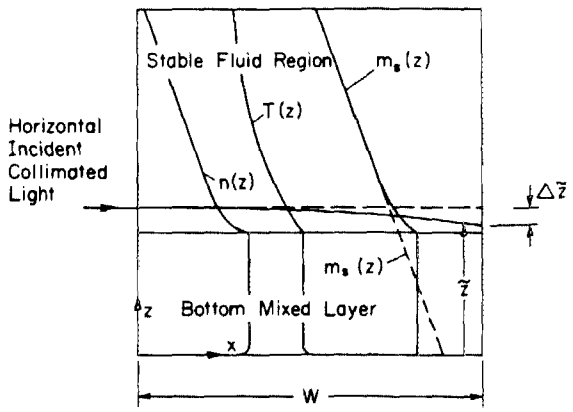

FIG. 1. Schematic of the salt-stratified system heated from below. The deflected and undeflected beams are shown as solid and dashed lines, respectively.

 0034-6748/86/102538-05$01.30

A thorough understanding of system behavior requires knowledge of the vertical salinity distribution, particularly in the interfacial region separating the mixed and stable layers. The salinity distribution may be inferred with optical techniques which measure the refractive index, n, of the fluid, if the fluid temperature, T, is independently determined. Accepted correlations which relate the salt mass fraction, m_s, to the temperature and refractive index of salt water[11] may be subsequently employed to evaluate the salinity distribution.

The optical technique used in this study measures $n(z)$ by monitoring the deflection of an initially horizontal light beam as it traverses the salt-stratified system. The trajectory of the light beam depends on $n(z)$ and is described by a modified, one-dimensional form of the Euler–LaGrange equation[9]

$$\frac{\partial^2 \tilde{z}}{\partial x^2} = \left[1 + \left(\frac{\partial \tilde{z}}{\partial x}\right)^2\right]\left(\frac{1}{n(z)}\frac{\partial n}{\partial z}\right), \tag{1}$$

where $\tilde{z}$ is the height of the beam trajectory and the coordinate system is shown in Fig. 1. Equation (1) may be integrated in the x direction to yield[9]

$$\Delta\tilde{z} = -\int_{x=0}^{W}\left[\left(\frac{n(\tilde{z})}{n(\tilde{z}(x=W))}\right)^2 - 1\right]^{1/2} dx, \tag{2}$$

where $\Delta\tilde{z}$ is the distance that the light beam is deflected downward after traversing the test cell width, W,

$$\Delta\tilde{z} \equiv \tilde{z}\,(x=0) - \tilde{z}\,(x=W). \tag{3}$$

Hence, if $\Delta\tilde{z}$ is known, $n(\tilde{z}) = n(z)$ may be determined. Details of the data reduction technique associated with this procedure are in the Appendix.

The experimental arrangement used in this study is illustrated in Fig. 2. A shadowgraph, consisting of a light source, condensing lens, pinhole, and collimating lens, was assembled. A test cell was inserted in the collimated shadowgraph beam, and a diffusing glass screen was placed against its outer wall. The deflection of the light beam was measured by placing a slanted wire (1–2 mm diameter) in the shadowgraph beam upstream of the test cell. The wire was oriented at an angle of approximately 45° from the horizontal, although the orientation of the wire is arbitrary when considering a one-dimensional refractive index distribution. The wire casts a shadow which is deflected as it propagates through the salt solution. The deflection is measured from photographs of the diffusing glass screen.

Two test cells were used. A small test cell[4] was constructed of 25-mm-thick acrylic sheet with base dimensions of 305×305 mm^2 and a wall height of 200 mm. A large test cell[12] was $660 \times 660 \times 660$ mm^3 and was constructed of 12.7-mm-thick tempered glass housed in a metal frame. The different test cell sizes required different shadowgraph arrangements which are described in Table I. Shadowgraph systems A and B were used with the small test cell, and system C was used in conjunction with the large test cell.

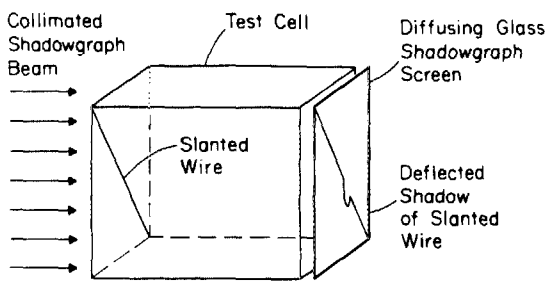

FIG. 2. Schematic of the experimental apparatus.

TABLE I. Shadowgraph systems.

System	Light source	Collimating lens
A	5-mW HeNe laser	90-mm-diam convex
B	Mercury arc	500×600 mm^2 plastic Fresnel lens
C	Mercury arc	200-mm-diam planoconvex

II. EXPERIMENTAL RESULTS

Three phases of experimentation were considered: (i) verification of the deflectometric and data reduction techniques by comparison with independent salinity measurements in an isothermal salt-stratified system, (ii) use of deflectometry to measure a salinity distribution in a double-diffusive system, and (iii) use of deflectometry in conjunction with shadowgraph flow visualization to provide a more meaningful interpretation of shadowgraphic results.

A. Phase I: Verification of the deflectometric technique

Shadowgraph system A was employed in the first phase of the experiments. The small test cell was filled to a height of 140 mm with two 70-mm-deep water layers of uniform salinity (0 and 14.5 wt. % NaCl). The top of the test cell was covered to minimize evaporative losses, and the salt diffusion process at the interface between the two fluid layers was simultaneously monitored with deflectometry and a vertically traversing fiber-optic refractometer.[4]

Figure 3 shows a series of shadowgraph/deflectometry results. Before filling the test cell, the shadow of the slanted wire propagates through the system without being deflected and is marked on the diffusing glass screen [Fig. 3(a)]. After the two fluid layers are introduced, the shadow of the wire is deflected downward by the refractive index gradient associated with the salinity gradient at $z = 70$ mm [Fig. 3(b)]. As salt diffusion continues [Figs. 3(c) and 3(d)], the maximum value of $\Delta\tilde{z}$ decreases, while the wire shadow deviates from its undeflected position at higher and lower z, indicating the establishment of salinity gradients away from $z = 70$ mm.

Deflection distributions were measured from Fig. 3 and were used to evaluate $n(z)$. The salinity distribution, $m_s(z)$, was subsequently determined with the relationships of Ruddick and Shirtcliffe.[11] A fiber-optic refractometer was used to independently measure $m_s(z)$, and the two salinity distributions are shown in Fig. 4.

The deflectometric salinity measurements (symbols) of

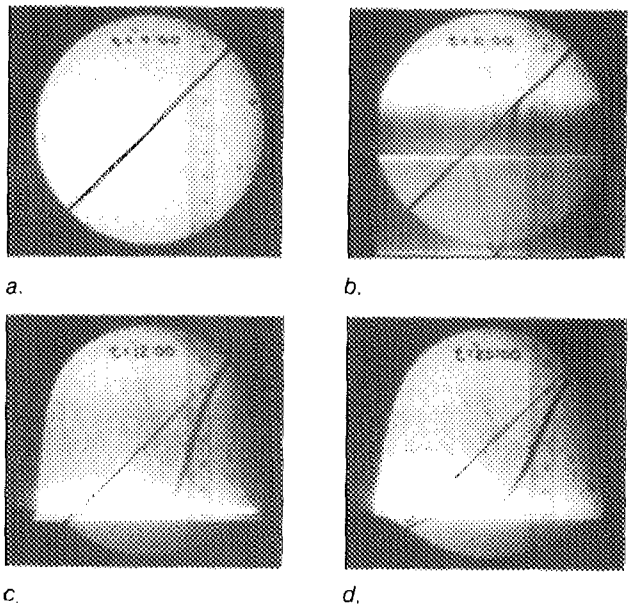

FIG. 3. Simultaneous shadowgraph and deflectometry results for the isothermal two-layer salt system (scale in cm).

Fig. 4 compare favorably with the refractometric measurements (lines) and the salinity distributions may be qualitatively explained in terms of the wire shadow deflections of Fig. 3. Maximum salinity gradients occur at $z = 70$ mm and correspond to the location of the maximum wire shadow deflections of Fig. 3. As the salinity distributions become uniform above and below $z = 70$ mm, the wire shadow deflections become small. The wire shadow deflections extend to the outer boundaries of the shadowgraphs' field of view as the salinity gradients propagate away from $z = 70$ mm.

Since the deflectrometric salinity measurements are in good agreement with the refractometrically obtained values, and since the behavior of the wire shadow deflections is expected, it is concluded that the deflectometry technique and data reduction routine described in the Appendix are valid.

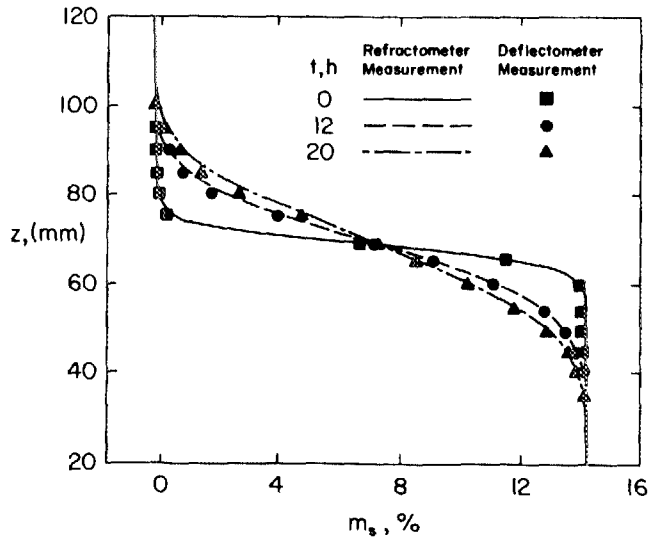

FIG. 4. Transient salinity profiles corresponding to the results of Fig. 3.

B. Phase II: Use of deflectometry under double-diffusive conditions

Although the results of Fig. 4 confirm the salinity measurement technique in isothermal fluids, the main purpose of this study is to consider use of deflectometry under double-diffusive conditions. Hence the large test cell, outfitted with shadowgraphic system B, was filled with a linear salinity distribution characterized by a salt gradient of 34.8%/m. The test cell walls were insulated with removable 50-mm styrofoam sheets and 300-mm fiberglass batting. The salt-stratified fluid layer was destabilized by an applied heat flux of 100 W/m^2. Because of bottom heating, a single mixed layer developed at the expense of the overlying stable fluid.[12]

After 12 days of continuous bottom heating, the mixed layer attained a height of approximately 275 mm. A shadowgraph of the interfacial region between the mixed and stable layers is shown in Fig. 5. Note that the interfacial region is denoted by a set of bright and dark shadowgraph bands between uniformly gray regions corresponding to the bottom mixed layer (uniform salinity) and the stable layer (uniform salinity gradient).

The deflected shadow of the slanted wire is also evident in Fig. 5, as is the undeflected shadow, which was applied to the photograph after the experiment. (The undeflected shadow in the uniform refractive index mixed layer was extrapolated into the overlying region.)

A comparison of the shadow images in Figs. 3 and 5 shows that, under double-diffusive conditions, evaluation of $\Delta\tilde{z}$ is more difficult because of shadow fluctuations at the bottom of the stable fluid layer. These fluctuations are due to local fluid motion in the interfacial region resulting from the bombardment of the stable fluid by thermal plumes ascending from the bottom heated surface of the test cell. Despite the difficulty in evaluating the precise shadow location in the interfacial region, $\Delta\tilde{z}$ can be estimated from Fig. 5. Time averaging the shadow with long exposure photography or temporarilly curtailing bottom heating may be used to eliminate shadow fluctuation.

Local fluid temperatures were also measured by traversing a thermocouple through the interfacial region of Fig. 5. As such, the refractive index distribution, obtained by deflectometry, may be used to evaluate the salinity distribution, $m_s(z)$, with knowledge of the independently measured

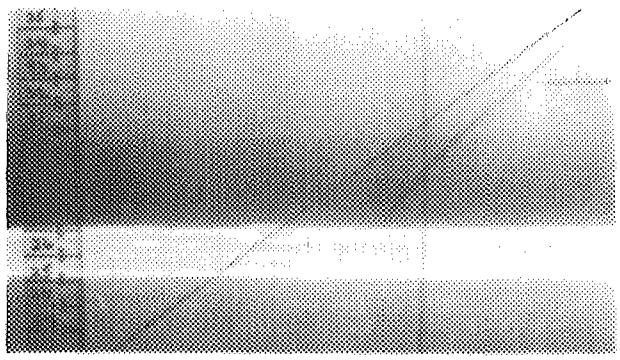

FIG. 5. Simultaneous shadowgraph and deflectometric results for the double-diffusive system heated from below in the large test cell (scale in cm).

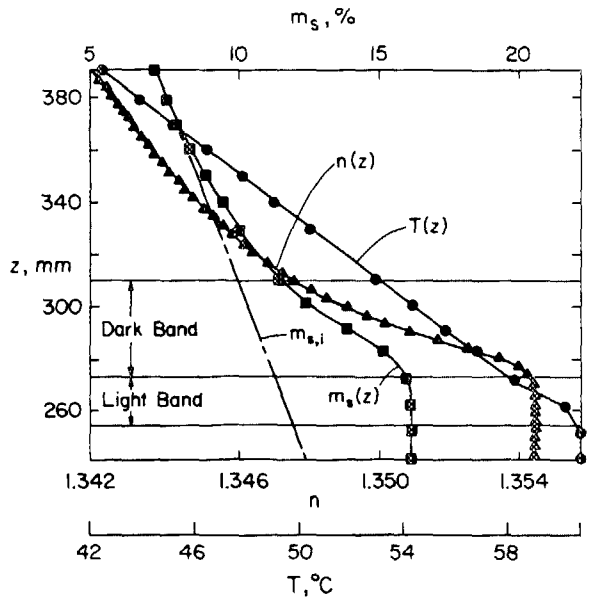

FIG. 6. Measured refractive index, temperature, and salinity distributions corresponding to the results of Fig. 5.

temperature distribution, $T(z)$. The refractive index, temperature, and salinity distributions corresponding to the shadowgraph of Fig. 5 are shown in Fig. 6. The unstable temperature distribution is nearly linear in the lower regions of the stable fluid layer, while the refractive index distribution is clearly nonlinear. As such, the salinity distribution must be nonlinear.

Figure 6 also shows the initial salinity distribution, $m_{s,i}$. Near $z = 380$ mm, the measured and initial salinity distributions are approximately equivalent. However, near the interfacial region ($z \approx 300$ mm), measured salinity gradients are larger, suggesting significant salt transport from the relatively high salinity bottom mixed layer. The salinity at $z \approx 270$ mm has increased because of mixing of the initial salinity distribution by convection in the bottom mixed layer. Information concerning the salinity gradient in and immediately above the interfacial region between the mixed and stable layers is necessary to validate theories dealing with the mechanisms responsible for mixed layer growth[13,14] since the salinity gradient suppresses the development of convective conditions throughout the fluid layer. Historically, such information has been difficult to obtain.

C. Phase III: Quantitative interpretation of shadowgraph results

Since shadowgraphic and deflectometry results are both presented in Fig. 5, a more quantitative interpretation of the shadowgraphic band structure may be made. It is clear by inspection of Fig. 5 that light which enters the test cell within the dark band region is deflected downward by the refractive index gradients associated with the salinity profile of Fig. 6. Conversely, light which enters the test cell in the bright band propagates through the cell without being deflected. As such, the banded shadowgraph intensity distribution may be used to locate the height of the bottom mixed layer, which

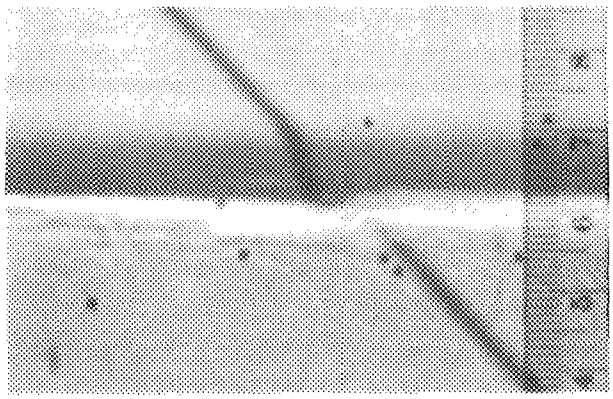

FIG. 7. Simultaneous shadowgraph and deflectometry results for the double-diffusive system heated from below in the small test cell (scale in cm).

corresponds to the interface between the bright and dark bands. Regions of steep salinity gradients are associated with the dark band, and the upper limit of the nonlinear salinity distribution in the bottom of the stable layer is associated with the top of the dark band.

Although the foregoing interpretation of the shadowgraph band structure does not provide the detailed salinity information which can be obtained by the deflectometric technique, it may still be useful in situations for which the sensitivity of deflectometry is limited. Inspection of Eq. (2) reveals that the deflection distance, $\Delta\bar{z}$, decreases with decreasing test cell width and refractive index (salinity) gradients. As such, salt-stratified double-diffusive experimentation performed in small tests cells with relatively small stabilizing salinity gradients may not permit successful utilization of the deflectometry method. To illustrate how the sensitivity of the technique varies with experimental conditions and test cell size, a series of experiments were performed in the small test cell with shadowgraph system C. Again, an initially linear salinity gradient was destabilized by bottom heating.[15]

A shadowgraph of the interfacial region is provided in Fig. 7. Experimental conditions correspond to an initial salinity gradient of 29.3%/m and a bottom heat flux of 450 W/m^2 and the shadowgraph was taken 6 h after initiation of bottom heating. For this relatively small salinity gradient and test cell width, the deflected wire shadow is not sufficiently distinct to determine $m_s(z)$. Wire shadow fluctuations are also more intense because of the higher bottom heating rate. However, it may be concluded from the previous discussion of Figs. 5 and 6 and, in particular, from interpretation of the banded shadowgraph intensity distributions, that the bottom mixed layer height is approximately 62 mm, while vertical penetration of the upward-diffusing nonlinear salinity distribution extends to approximately 70 mm.

III. DISCUSSION

The optical deflectometry technique has been used to determine salinity distributions in a double-diffusive thermohaline system. However, because of limitations in its sen-

sitivity, the deflectometry technique is not recommended for small test cells with small salinity gradients. Increased sensitivity may be accomplished, however, by moving the diffusing glass screen away from the test cell and the technique may be extended to two-dimensional systems by replacing the slanted wire with a grid. The three-dimensional Euler–LaGrange equations[9] would need to be solved to evaluate the two-dimensional refractive index distribution.

ACKNOWLEDGMENTS

The authors would like to thank the National Science Foundation for support of this work under Grants No. CBT 8552806 and No. CBT 8316580. Computational facilities were provided by the Department of Mechanical Engineering at The University of Texas, Austin.

APPENDIX

Equation (2) may be solved for the refractive index distribution within the system. However, approximate methods must be employed and are most easily applied by considering Eq. (1), which may be integrated to yield[9]

$$1+\left(\frac{\partial \tilde{z}}{\partial x}\right)^2=\left(\frac{an}{n_i}\right)^2, \tag{A1}$$

where

$$a\equiv\left\{1+\left[\left(\frac{\partial \tilde{z}}{\partial x}\right)_i\right]^2\right\}^{1/2}. \tag{A2}$$

Equation (A1) may, in turn, be integrated and rearranged to obtain[9]

$$\tilde{x}=\int_{z_i}^{\tilde{z}}\left[\left(\frac{an}{n_i}\right)^2-1\right]^{-1/2}dz, \tag{A3}$$

where $\tilde{x}$ is the horizontal propagation associated with a particular light beam elevation, $\tilde{z}$, and subscript i denotes initial conditions for the beam entering the calculation domain.

The fluid layer is divided into a number of calculation domains, each of height dz, and a piecewise linear refractive index distribution is assumed, as shown in Fig. 8. The calculation procedure begins in a fluid region of known n (the dz associated with the top of the bottom mixed layer with refractive index, n) and marches upward through the refractive index distribution. The adjacent, overlying nodal refractive index, n_2, is initially guessed and Eq. (A3) is solved for $\tilde{z}$ ($x=W$) until the measured $\Delta\tilde{z}$ is estimated to within 10^{-5} m. The process continues for all k nodes, solving for $n_3, n_4, \ldots, n_k$.

For large $\Delta\tilde{z}$, several dz elements may be crossed, as shown in Fig. 8. In this case, the test cell width is divided into regions of width L_j and subscript i is now associated with entering beam conditions for dz_{j-1}. The refractive index, n_j, is adjusted and Eqs. (A1)–(A3) are solved until $\tilde{z}$ ($x=W$) $\approx \tilde{z}$ ($x=0$) $-\Delta\tilde{z}$. The test cell wall thickness was ignored in all calculations and the polynomial curve fits of Ruddick and Shirtcliffe[11] were extended beyond their reported range of application. Neglecting the wall thickness of the test cell can lead to serious error in small test cells; however, extension of the polynomials of Ruddick and Shirtcliffe is not expected to produce large errors due to the nearly linear relationship between the fluid refractive index with salt concentration and temperature.

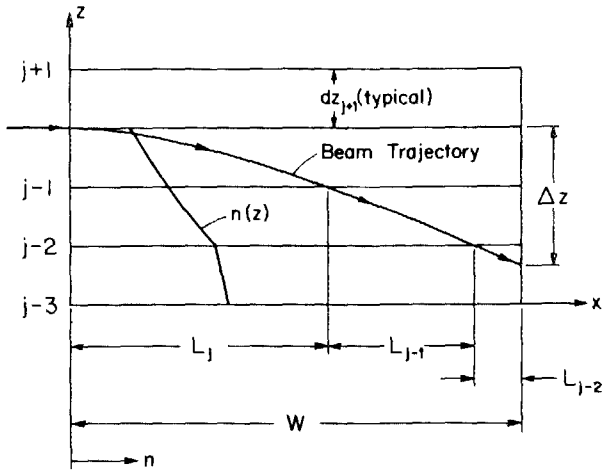

FIG. 8. Schematic of the individual calculation domains used in the data reduction routine.

An error analysis was performed on the measured salinities of Fig. 6. The uncertainty in the refractive index at $z=38.5$ mm, δn_k, was evaluated from[16]

$$\delta n_k=\left[\left(\frac{\partial n_k}{\partial\Delta\tilde{z}_1}\delta\Delta\tilde{z}_1\right)^2+\left(\frac{\partial n_k}{\partial\Delta\tilde{z}_2}\delta\Delta\tilde{z}_2\right)^2+\cdots+\left(\frac{\partial n_k}{\partial\Delta\tilde{z}_k}\delta\Delta\tilde{z}_k\right)^2\right]^{1/2}. \tag{A4}$$

The $\partial n/\partial\Delta\tilde{z}$ values were obtained by varying the individual $\Delta\tilde{z}$ quantities in the data reduction routine and monitoring the change in n_k. The uncertainty in the deflection, $\partial\Delta\tilde{z}$, was estimated as 2 mm. The resulting uncertainty in n_k is ± 0.0002 corresponding to an uncertainty in m_s of approximately $\pm 0.1\%$. The accuracy of the deflectometry technique deceases as W or the salinity gradient are decreased.

[1] J. S. Turner, *Buoyancy Effects in Fluids* (University of Cambridge, Cambridge, 1979).
[2] S. Martin and P. Kauffman, J. Fluid Mech. **64**, 507 (1974).
[3] D. P. Grimmer, G. F. Jones, G. F. Tafoya, and T. J. Fitzgerald, Rev. Sci. Instrum. **54**, 1744 (1983).
[4] T. L. Bergman, F. P. Incropera, and W. H. Stevenson, Rev. Sci. Instrum. **56**, 291 (1985).
[5] C. J. Poplawsky, F. P. Incropera, and R. Viskanta, J. Sol. Energy Eng. **103**, 351 (1981).
[6] W. T. Lewis, F. P. Incropera, and R. Viskanta, J. Fluid Mech. **116**, 411 (1982).
[7] W. L. Howes and D. R. Buchele, J. Opt. Soc. Am. **56**, 1517 (1966).
[8] F. J. Weinberg, *Optics of Flames* (Butterworths, London, 1963).
[9] D. E. Mowbray, J. Fluid Mech. **27**, 595 (1967).
[10] H. E. Huppert and P. F. Linden, J. Fluid Mech. **95**, 431 (1979).
[11] B. R. Ruddick and T. G. L. Shirtcliffe, Deep Sea Res. **26**, 775 (1979).
[12] D. R. Munoz, MS. thesis, Purdue University, West Lafayette, IN, 1983.
[13] K. A. Meyer, J. Sol. Energy Eng. **105**, 341 (1983).
[14] F. Zangrando, J. Green, and E. Fisher, American Institute of Chemical Engineers Symposium Series **80**, 452 (1984).
[15] T.L. Bergman, F. P. Incropera, and R. Viskanta, J. Heat Transfer **108**, 206 (1986).
[16] S. J. Kline and F. A. McClintock, Mech. Eng. **75**, 3 (1953).